PHYSICAL REVIEW B VOLUME 52, NUMBER 8 15 AUGUST 1995-II

Mechanistic study of atomic desorption resulting from the keV-ion bombardment of fcc{001} single-crystal metals

S. W. Rosencrance, J. S. Burnham, D. E. Sanders,* C. He, B. J. Garrison, and N. Winograd
Department of Chemistry, The Pennsylvania State University, University Park, Pennsylvania 16802

Z. Postawa
Jagellonian University, Institute of Physics, Reymonta 4, 30-059 Krakow, Poland

A. E. DePristo
Department of Chemistry and Ames Laboratory, Iowa State University, Ames, Iowa 50011

(Received 3 April 1995)

Energy-resolved angular distributions of Ni and Rh atoms desorbed by keV Ar^+ ion bombardment have been measured using multiphoton resonance ionization detection. The experimental spectra were simulated using molecular-dynamics calculations which are based on the molecular-dynamics/Monte Carlo corrected effective-medium interaction potential. Important collision events were identified using a recently developed graphical utility which allows easy visualization of atomic motions subsequent to bombardment. Three major microscopic ejection mechanisms were determined, each of which is categorized into three additional interactions. The features which make up the polar angle spectra are assigned to one of these mechanisms. We find that the majority of particles eject due to a collision with an atom from one layer below (Δ_1 mechanism). A mechanism involving a collision due to an atom from the same layer, however, is responsible for a shift in peak position with energy. This investigation strongly reinforces the view that the inherent registry of the atoms in the crystal lattice is the crucial factor in determining the dominant microscopic sequences of events which lead to ejection as well as the macroscopically observable quantities.

I. INTRODUCTION

The anisotropy present in the angular distributions of particles ejected from keV ion-bombarded single-crystal surfaces was observed in the mid-1950's by Wehner.[1] This discovery raised several interesting questions regarding the fundamental mechanisms responsible for the sputtering process. In the following years, experimental and theoretical work ensued from which many concepts were developed to explain the preferential ejection of particles along the various low-index crystallographic directions.[2] For instance, Silsbee proposed that the characteristic spot patterns[3] obtained were a result of focused collision sequences.[4] These focused collision sequences were assumed to originate many layers beneath the surface and act as an efficient means of momentum transport along the various closed-packed directions of the crystal lattice. About a decade later it was suggested by Harrison, Johnson, and Levy[5] as well as Lehman and Sigmund[6] that the peaks in the angular spectra need not necessarily be attributed to focused collision sequences and that the surface structure in the top few layers of the solid ultimately determined the resulting experimentally observable quantities. These original contributions, in combination with recent investigations, have been useful in unraveling the microscopic processes which lead to ejection following keV-ion bombardment of solid surfaces.[7–12]

One of the major advances in fundamental mechanistic investigation has been the ongoing development of molecular-dynamics (MD) computer simulations. Because these calculations are based on classical mechanics, the nuclear motions of the particles are inherently accessible. A large number of trajectories or individual collision cascades, each corresponding to the motion of several hundred atoms, however, must be evaluated to obtain sufficient sampling statistics. The extraction of mechanistic information from this large volume of data has proven to be tedious, time consuming, and extremely difficult, largely because each motion must be examined by eye and could not be automated. Several extraction methods have been employed previously,[13–20] each yielding a degree of success. All are still time consuming to prepare, computer disk intensive to retain, and difficult to analyze. Recent advances in the speed of computers, however, in tandem with more sophisticated graphics software have made it possible to reopen the question of whether it is possible to trace and mechanistically deconvolute each and every desorption event from a large number of individual collision cascades.[21]

The purpose of this work is to address some of the persisting questions concerning the mechanistic details of atomic desorption from fcc{001} single-crystal metals. Among these concerns are the mechanisms of ejection for different fcc{001} materials and the events that are universal for the fcc{001} crystal face of metal surfaces. Also of interest is the importance of focused collision sequences to the overall sputter yield and angular distribution.

To accomplish this goal, we have measured the

0163-1829/95/52(8)/6006(9)/$06.00

kinetic-energy and angle-resolved distributions of neutral particles ejected from Ni{001} and Rh{001} due to 5 keV Ar^+ ion bombardment. Rhodium and nickel were chosen as Rh is 75% more massive than Ni and the Rh lattice constant is 8% larger than that of Ni. In addition to the experimental measurements, we have performed molecular-dynamics simulations of the collision events for each system. A recently developed graphical utility, which allows visualization of the space-time evolution of collision mechanisms, was used to systematically investigate the trajectories of every particle ejected within a statistically valid set of trajectories.[21] The motions are then categorized by type of mechanism. This deconvolution procedure allows us to statistically evaluate the significance of the recurring events that lead to ejection. Furthermore, we provide both a qualitative and a quantitative description of the processes which contribute to the structure in the angular spectra.

We find that the majority of particles eject, due to a collision with atom from one layer below (Δ_1 mechanism). A mechanism involving a collision due to an atom from the same layer, however, is responsible for a shift in peak position with energy. This investigation strongly reinforces the view that the inherent registry of the atoms in the crystal lattice is the crucial factor in determining the dominant microscopic sequences of events, which lead to ejection as well as the macroscopically observable quantities.

II. EXPERIMENT

The experimental apparatus is described briefly as it has previously been extensively detailed.[22] The ultrahigh-vacuum (UHV) chamber (2×10^{-10} torr base pressure) is equipped with low-energy electron diffraction (LEED), retarding grid electron optics for Auger analysis, as well as an energy and mass filtered ion source capable of operating in either pulsed or continuous mode. To initiate the experiment, a 250-ns pulse of 5 keV Ar^+ ions is focused onto a well-defined 2-mm spot on the single-crystal surface. A variable delay tunable dye laser pulse is focused into a narrow ribbon, which selectively ionizes ejected neutral atoms, thus defining the translational energy by the corresponding velocity time of flight. These ions then enter a series of ion optics and eventually impinge upon a position sensitive microchannel plate (MCP). The amplified ion signal exiting the rear of the MCP impinges on a biased phosphor screen. The resulting image is monitored by a video camera and sent to a video processing module interfaced to a personal computer. The information thus obtained is deconvoluted into an energy and angle-resolved photoion map through software developed in our laboratory.

The samples used in these experiments are optically polished single crystals of nickel and rhodium oriented to within ±0.5° of the {001} surface plane. The Ni crystal was extensively cleaned by a series of sputtering (5-keV Ar^+, 5 mA/cm^2, 30 min) and annealing (920 K, 30 min) cycles. Flashing the crystal to 1100 K resulted in a bright, sharp (1×1) LEED pattern. The cleaning procedure of Rh is similar to that for Ni, except that it was exposed at 1100 K to oxygen (1×10^{-7} torr, 20 min) and hydrogen (1×10^{-7} torr, 20 min) previous to the flash of 1400 K to obtain the sharp (1×1) LEED pattern.

III. SIMULATION

The molecular-dynamics scheme has been described in detail elsewhere.[23–27] Briefly, the classical equations of motion are integrated in time using an interaction potential that describes the system of interest. The final velocities are used to calculate kinetic-energy and angular distributions. The time evolution of the atomic motions is used to extract the important collision events.

The interaction potential used for both Ni and Rh is the molecular dynamics/Monte Carlo corrected effective-medium (MD/MC-CEM) potential.[28,29] The interaction energy, ΔE, of the entire system in MD/MC-CEM potentials is written as

$$\Delta E=\Sigma\Delta F_J(A_i;n_i)+\tfrac{1}{2}\Sigma_i\Sigma_j V_c(A_i,A_j) ,$$

where the set of atoms is $\{A_i, i=1,N\}$. The jellium density, n_i, is

$$n_i=\frac{1}{2}\sum_{j\neq i}^{N}\int\frac{n(A_i;\mathbf{r}-\mathbf{R}_i)}{Z_i}n(A_j;\mathbf{r}-\mathbf{R}_j)\,d\mathbf{r} ,$$

where $n(A_i;\mathbf{r}-\mathbf{R}_i)$ is the atomic electron-density distribution as taken from Hartree-Fock calculations[30,31] and represented in even-tempered Gaussians[32] for computational ease. Z_i and R_i are the atomic number and nuclear position, respectively. The term ΔF_J is an empirical embedding function designated to ensure that the expression describes the properties of the atom in bulk and diatomic environments. The last term V_c is the Coulombic interaction between atoms A_i and A_j. This term is calculated directly from the specified atomic electron densities given by the Hartree-Fock calculations. The overlaps and Coulomb integrals are evaluated on a fine evenly spaced grid in $1/R^2$ and evaluated by a table look up for computational efficiency. More details about the implementation can be found in Ref. 33.

The only term adjusted to experimental data is the empirical embedding function ΔF_J. The interaction energies for Rh, Al, and the group-VIII elements are fit to bulk properties, as well as dimer properties.[34,35] Another feature of the MD/MC-CEM potential is that it obeys reasonable behavior at small internuclear separations. These two features make it attractive to switch from the embedded-atom method (EAM) potentials[36–38] that we had been using. The developers of these EAM potentials were interested in bulk equilibrium properties and did not place a priority on describing the dimer stability nor the energetics at a small internuclear separation. These EAM potentials[36–38] for the group-VIII metals as well as our own Rh potential[26] overbind most of the dimers by a factor of 2. To correct for the lack of a sufficiently repulsive interaction at small internuclear separations, we have in the past splined a Moliére potential to the EAM potential.[39] A Moliére potential, however, was used to describe Ar-Ni and Ar-Rh interactions.[40]

The theoretical model approximates the Ni{001} and

Rh{001} surfaces by a microcrystallite of 1800 atoms arranged in nine layers of 200 atoms each. This crystal size is chosen such that the energy and angular distributions are the same as with a larger crystal. The initial positions of the atoms are the bulk equilibrium positions and the solid atoms have zero initial kinetic energy. Each trajectory is initiated by an Ar particle with 3 keV of kinetic-energy bombarding the surface at normal incidence. Open boundary conditions are used as particles that leave the sides and bottom of the crystal in reality penetrate deeper into the crystal. The trajectories are terminated when the most energetic particle remaining in the solid has insufficient energy to overcome its attractive interactions to the solid.

The experimental data are an average over many collision cascades or individual Ar impacts on the surface. Similarly, the calculations must also be performed for the entire surface. Since the surface has translational and rotational symmetries, it is possible to reduce the impact region to a triangular impact zone near the center of the crystal.[7] In order to establish whether our results are statistically converged, we computed a total of ten individual sets of Ar impacts, in which each set consist of 150-Ar impacts randomly chosen within the triangular impact zone. After each set of 150 trajectories, we examined the energy and angular distributions in order to assess the convergence. The main features in the distributions are present even in one set of 150 trajectories. Consequently, for the mechanistic analysis, we use one of these 150 trajectory sets. The essence of the method developed by Sanders *et al.*[21] is that the mechanism of ejection for every atom in this 150 trajectory set (~450–500 atoms for each Ni and Rh) can be determined. The 1500 trajectory set is used to further increase the signal to noise ratio.

The essential information for the graphs of the motion is determined by a method developed by Harrison,[41] which is termed "lean-on," a colloquial expression for a collision. If only pair potentials are used for the interactions among the atoms, it is relatively straightforward to define a collision to be when two atoms have potential energy greater than a specified value, typically slightly greater than zero. Past experience using this definition shows that it highlights the key factors for atomic motion, except for changes in direction driven by attractive interactions, e.g., the pull of an atom towards the surface as it ejects. Ambiguity results when attempting to adapt this definition to many-body potentials as the energy is no longer simply a function of the positions of two atoms, but rather depends also on the positions of other nearby atoms. To obtain the information required, we have arbitrarily decided to use a repulsive Moliére potential[40] to define a collision. Thus, at each integration step, we check to see if the Moliére interaction between a pair of atoms is greater than a threshold value, in this case 10 eV. If this is true, then we flag the event as a collision within the lean-on tree. We must emphasize that there is some latitude in both the choice of the Moliére potential and the threshold value. If, in fact, the mechanistic interpretation of the important collisional events appears to be too sensitive to this arbitrary definition, then the atomic motions must be examined more carefully. In particular, low-energy motions are often influenced by attractive interactions, which would not be flagged as collision.

For each trajectory in the simulation, a lean-on tree is determined. Initially the primary Ar particle strikes one of the substrate atoms, then each of these two species can undergo further collisions. At each integration step, the positions and velocities are saved for only the atoms that are part of the lean-on tree. For example, at the first integration step the initial positions are saved. Once the Ar atom collides with another substrate atom, the positions and velocities of these two atoms are saved at *all subsequent* steps. Once an atom becomes part of the tree it is not removed even though it may no longer be colliding with another atom. The quantity of information is greatly reduced by saving only the step information of atoms that undergoes collisions. This lean-on analysis has no influence on the integration process.

After calculation and analysis of all trajectories, a set of atoms that has ejected is chosen for use in mechanistic elucidation. Since the atom number and trajectory number are known, we have written a program that scans through the saved information and extracts the positions and velocities of the atoms involved in the momentum-transfer sequence, which eventually ejects the atom of interest.

IV. RESULTS AND DISCUSSION

In the first section of our discussion a comparison of both the experimental and the calculated angular spectra of Ni and Rh are presented as well as a brief quantitative analysis of the effect of surface geometry on the trajectory of an ejecting atom. In the final part of the discussion, the various ejection mechanisms are discussed. Moreover, the relative abundances and angular contributions of these mechanisms are presented. A universal picture of ejection from fcc{001} metals is developed and quantitative information regarding the activity of focused collision sequences subsequent to bombardment of the {001} crystal face is presented.

A. General features

The general focus of this investigation is to complete a mechanistic study of the ejection processes as a function of kinetic energy and take-off angle. Consequently, we have plotted energy resolved polar angle distributions for the open ⟨100⟩ and the close-packed ⟨110⟩ azimuthal directions shown in Fig. 1. The experimental and calculated polar distributions for the Ni ($^3D_3$) (Ref. 42) and Rh ($^4F_{9/2}$) (Ref. 43) fine-structure states are shown in Figs. 2 and 3, respectively. As analyzed previously,[43] all the distributions are characterized by three regions of high intensity or peaks. There is a peak in the direction normal to the surface ($\theta=0°$) and two off-normal peaks, one in each azimuthal direction. The most intense peak is along the open ⟨100⟩ azimuth. For both Ni and Rh, the experimentally determined peak position is ~50° for the 5–10-eV particles. As the energy increases, the peak

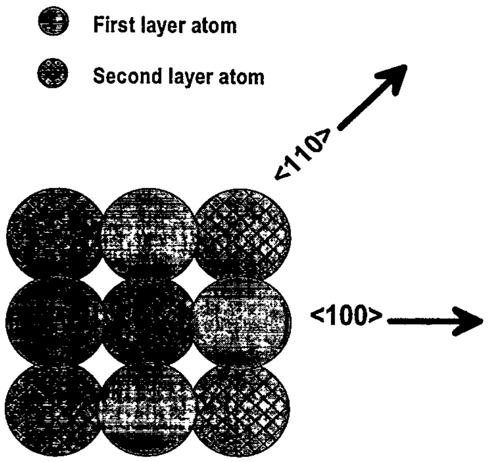

FIG. 1. Pictorial representation of the {001} surface plane. Light shaded atoms are in the first layer and dark shaded atoms are in the second layer. Azimuths of the discussion are denoted by arrows.

moves toward the surface normal. Along the ⟨110⟩ direction the off-normal peak is observed at ~35°. The last peak is in the direction normal to the surface. Since the distributions plotted in Figs. 2 and 3 have not been corrected for solid acceptance angle, the actual intensity of the peak normal to the surface ($\theta=0°$) is smaller than shown. This is not significant, however, for the following discussions.

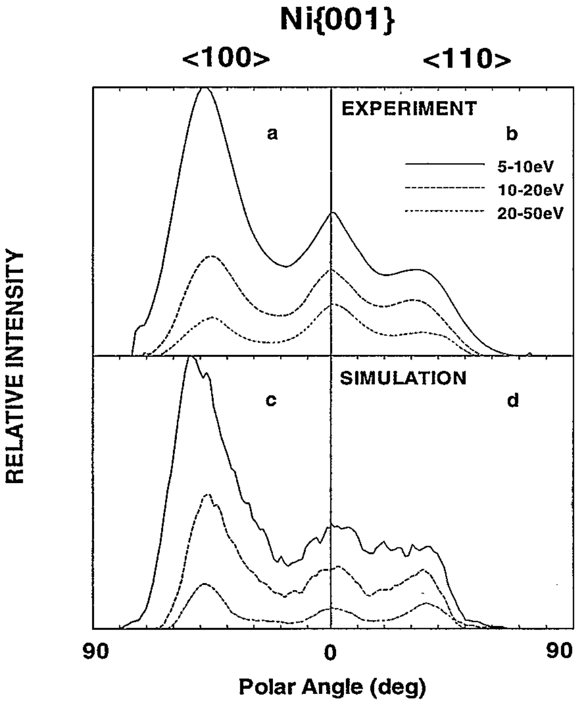

FIG. 2. Experimentally measured (top) and calculated (bottom) polar angle distributions for Ni for three energy ranges of ejected particles. (a) and (c) are for the open ⟨100⟩ azimuth and (b) and (d) are for the close packed ⟨110⟩ azimuth. These plots have not been adjusted for a solid angle. Consequently the peak at normal ejection ($\theta=0°$) appears more prominent than it actually is.

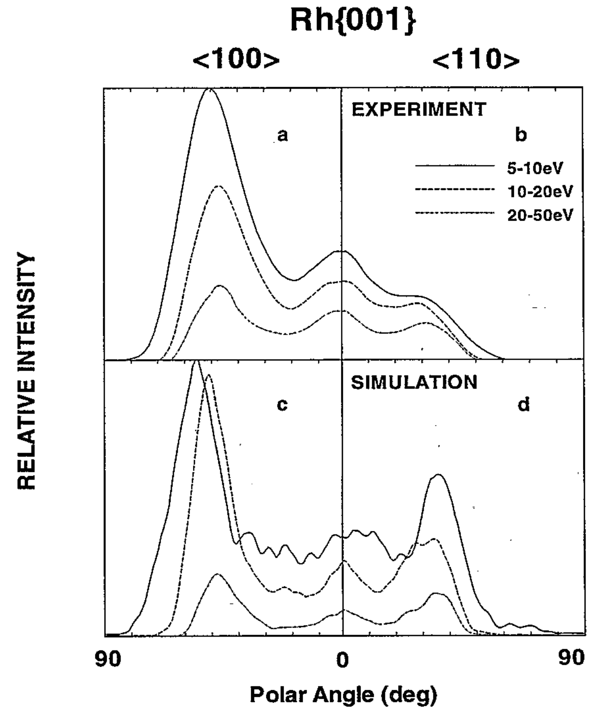

FIG. 3. Experimentally measured (top) and calculated (bottom) polar angle distributions for Rh in the same format as for Ni in Fig. 2.

The similarity between the Ni and Rh experimental distributions is striking. The main difference is that the Rh energy distribution peaks at a slightly higher value (~5 eV) than Ni (~4–4.5 eV). Consequently, there are relatively more particles in the Rh higher-energy ranges.

The calculated distributions generally exhibit the same features and trends as the experimental distribution. Of special significance is that the MD/MC-CEM potentials were developed prior to performing these experiments and no adjustment of the potential has been made. As a consequence, we are confident that these calculations provide an excellent set of trajectories that can be used for a mechanistic analyses of the ejection process.

The main difference between the Rh{001} calculated results using the MD/MC-CEM potential and those published[43] using the EAM potential[26] is that the EAM potential predicts that the intensity at $\theta=0°$ for 5–10-eV particles is greater than the intensity at $\theta=50°$ in the ⟨100⟩ azimuth. Remarkably the MD/MC-CEM potential improves the agreement with experimental data. Both potentials predict a larger intensity at $\theta=40–50°$ in both the ⟨100⟩ and ⟨100⟩ directions than is observed in the experimental data.

Before presenting specifics of the ejection mechanisms, some global analysis of the yields is appropriate. The total yields as well as the monomer yields are given in Table I. The yields for Ni are higher than for Rh, which is expected because Ni has the lower cohesive energy. As found in previous studies,[44] the majority of the ejected species originate from the first layer.

Although there is only a small component of second-layer atoms in the overall ejection statistics, it has been suggested that these species could contribute significantly

TABLE I. Ejection yields. Yield is the number of ejected particles per impinging projectile ion. A total of 1500-Ar impact points were calculated. The percentage of ejected yield per layer is for monomers only.

	Ni{001}	Rh{001}
Yield (Total)	4.12	3.56
Yield (Monomer)	3.88	3.30
Layer 1	86%	91%
Layer 2	12%	8%
≥ Layer 3	2%	1%

in the normal direction ($\theta=0°$) of ejection.[10,45] The calculated layer-resolved energy-integrated angular distributions of Ni and Rh are shown in Fig. 4. We find for Ni and Rh that 55% and 34%, respectively, of the atoms, which eject at polar angles of less than 10°, originate from the second layer of the lattice. Hence, it is likely that the ejection of second-layer atoms are important for this geometry. This effect could be experimentally investigated using layered bimetallic systems[46] as targets, in tandem with the sensitivity of laser postionization detection.

B. Mechanistic evaluation

In this section, the microscopic mechanisms of desorption are presented. We find that the mechanisms can be classified based on the number of layers between the original position of the ejecting species and the particle, which via collision, gives the ejecting particle sufficient translational energy to eject.[21]

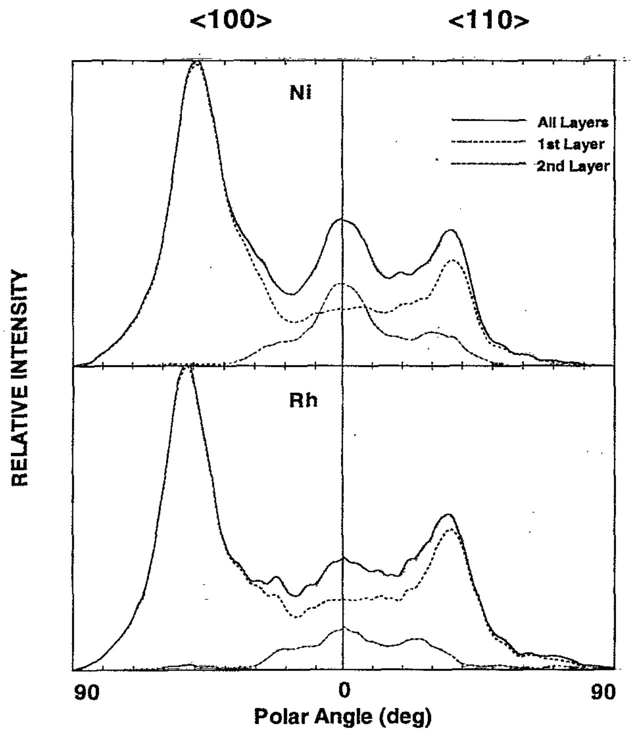

FIG. 4. Calculated polar angle distributions vs layer of origin of the atoms. The distributions are for atoms with 0–50 eV of kinetic energy.

Pictorial representations of the events preceding ejection, shown in Fig. 5, have been used to trace the path of momentum transfer after ion impact and to categorize the events which lead to ejection. Each plot has two parts, the first being many atoms in their initial positions (prior to bombardment) and the second being the positions of the three trace atoms shown at 5-fs (1 fs $= 10^{-15}$ s) intervals. The radius of the trace atoms is proportional to their instantaneous total (kinetic+potential) energy. The fixed crystal atoms are drawn with a radius which is equivalent to 40 eV of total energy. This graphical representation depicts the time dependence of the positions and energy of the trace atoms in a compact form. Moreover, the motions of the remainder of the atoms are not shown and thus do not visually detract from the motions of the particles of interest. The advantage of this graphical representation is that the picture is sufficiently simple that virtually all the ejection events can be viewed in order to obtain a perspective of the important collisions. The disadvantage is that a false impression is given that only a few atoms are moving during the ejection sequence. This latter conclusion is not correct and, in fact, many atoms have moved from their original positions.

Plots of the three most common mechanisms of ejection are shown in Fig. 5. The Δ_0 ejection mechanism results when the momentum transfer that leads to desorption is from an atom in the same layer as the ejecting particle as shown in Fig. 5(a). Here, the second particle from the right in the first layer is energized, most likely via interaction with the projectile, and transfers a portion of this energy to the species directly to its left. The momentum transferred is sufficient to overcome the surface binding energy and the particle ejects into the vacuum. The atom is then deflected towards a more normal direction, due to a collision with a neighboring atom. The second major recurring ejection event is the Δ_1 mechanism. In this case, the collision which leads to ejection is with a particle in the layer directly below that of the desorbing particle. More specifically, the Ar projectile deposits a portion of its initial momentum several layers below the surface. The momentum can transfer back to the surface in a sequence, shown in Fig. 5(b), whereby the energized second-layer atom interacts with a first-layer particle leading to ejection. The final significant mechanistic subdivision is the Δ_2 mechanism. A Δ_2 mechanism occurs when a particle two layers away from its eventual collision partner moves through the lattice and ejects a particle [Fig. 5(c)]. Subsequent to initial momentum deposition by the projectile, a particle in the third layer is activated and moves towards the surface. This particle collides with a particle in the first layer and ejects it into vacuum. We found during our quantitative analysis that Δ_n processes rarely occur when n is greater than two. This is in contrast to Si{001} in which the Δ_3 mechanisms are quite common due to the openness of the Si lattice.[21]

The calculated contributions of the various Δ events for Ni and Rh are shown in Table II. For both metals, it is clear that the Δ_1 processes are dominant, contributing to 75%±8% of the ejection yield for Ni and 84%±8% for Rh. Compared to the number of Δ_1 interactions, the relative amount of Δ_0 and Δ_2 events is small. With the exception of a slight redistribution of the Δ_2 mechanism into the Δ_1 channel for the Rh case relative to the Ni case, the majority of Δ processes are very similar for both materials.

Peak normalized distributions of the various Δ processes plotted as a function of the ejecting particles initial lateral distance from the origin of the impact zone are shown in Fig. 6. For instance, all ejecting particles whose original lateral lattice position is up to and including one lattice constant (a_o) from the impact origin are included in the first data point. This first bin also contains the particle located at the impact origin even though it seldom ejects. All ejected particles originating from a lateral distance greater than na_o up to values less than or equal to $(n+1)a_o$ are plotted as the $(n+1)$ point, etc. As is evidenced in this plot, Δ_0 events typically occur very close to the point of impact. This short-range character arises because most of these sequences are initiated by the grazing interaction between the incident projectile and a first-layer atom. The Δ_1 and Δ_2 processes occur farther from the impact point and are typically initiated via momentum transfer, which has been redirected toward the surface from the original collision point several layers deep into the bulk. The remarkable similarity in the distributions of the Δ processes for both Ni and Rh implicates the innate structure of the fcc{001} crystal is a primary factor in governing the microscopic events leading to desorption. This similarity as well as those presented earlier allow us to simplify the discussion and concentrate from this point on one of the metals, namely Ni.

The inherent structure of the lattice also directly affects the relative angular contributions of the various Δ processes. The energy-integrated angular spectra of the various Δ events for Ni are shown in Fig. 7. For the off-normal peak in the open ⟨100⟩ azimuth, Δ_1 events dominate and particles that eject via this mechanism peak at about the same angle as the total distribution. The particles from the Δ_2 and Δ_0 events peak at an angle closer to the surface normal. The energy dependence is such that the Δ_1 events result mostly in emitted particles with kinetic energy <20 eV. The energy distribution of the Δ_0 events peaks in the 10–20 eV range and is almost entirely responsible for the intensity in the 20–50-eV range. It is the Δ_0 mechanism that is responsible for the shift in peak position as the energy increases. Finally, particles that eject via the Δ_2 mechanism have kinetic energies <20 eV. Since the number of particles that eject due to this mechanism is small compared to the Δ_1 mechanism, there is no discernible feature in the polar distributions that can be ascribed to the Δ_2 mechanism.

Similar trends hold for the off-normal peak in the ⟨110⟩ direction. Particles that eject via the Δ_1 mecha-

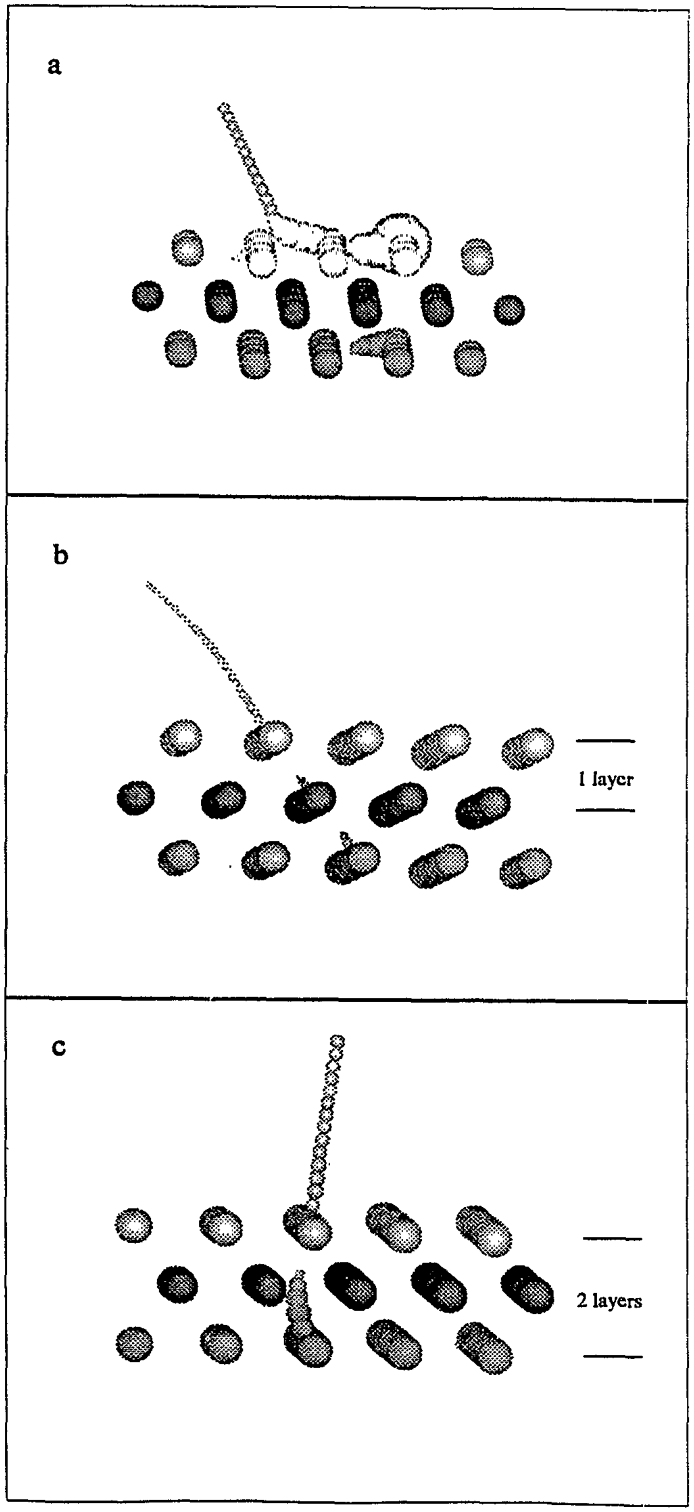

FIG. 5. Time lapse representation of trajectories leading to ejection of atoms from a fcc{001} surface. Only the motion of the last three atoms in the collision sequence is shown. Sizes of the moving atoms reflect their instantaneous total (kinetic+potential) energy and their positions are plotted at 5-fs intervals. The diameter of the rigid crystal atoms is equivalent to a 40-eV total energy. The view is from the $\langle 0\bar{1}0\rangle$ direction. The atoms are shaded by layer position in the surface. (a) Δ_0 mechanism. The atom that ejects is in the same layer as the atom that energizes it. (b) Δ_1 mechanism. The atom that ejects is one layer above the atom that energizes it. In this case, the trajectory depicted is a focused collision sequence of length 2. (c) Δ_2 mechanism. The atom that ejects is two layers displaced from the collision partner. In this case, the third-layer atom is energized by a Δ_1 mechanism.

TABLE II. Percentage of ejected atoms resolved by ejection mechanism. Shown are the results of our analysis for 150 trajectories, which were mechanistically categorized using our graphical "lean-on" method.

	Ni{001}			Rh{001}		
	Δ_0	Δ_1	Δ_2	Δ_0	Δ_1	Δ_2
NNE (Direct)	2%	23%	6%	7%	26%	3%
NNE (Grazing)	6%	40%	7%	4%	51%	3%
non-NNE	2%	11%	2%	<1%	7%	<1%
Total	10%	75%	15%	10%	84%	6%

nism generally have kinetic energies <20 eV and are responsible for the peak (or shoulder) in the 5–10 and 10–20-eV ranges. The particles that eject via the Δ_2 mechanism also have low energies, but there is negligible intensity compared with Δ_1. The Δ_0 events again peak in the 10–20-eV range. For the 20–50-eV range, the small intensity in the off-normal peak has contributions from all mechanisms, although Δ_0 is the dominant mechanism.

Finally, there is the peak in the direction normal to the surface. In the 5–10 eV range the Δ_1 events dominate, in the 10–20-eV range the Δ_2 events dominate, and in the 20–50-eV range the Δ_1 events again dominate. The Δ_2 ejection events in the 10–20-eV range quite clearly arise from atoms from two layers below moving more or less straight up and pushing the other atom straight up. In this 10–20-eV range, there are no atoms ejected normal to the surface, due to the Δ_1 mechanism, yet there are atoms ejected at lower and higher energies. This discontinuity implies that the mechanisms can be further subdivided.

The Δ processes can be divided into three more specific mechanisms. Interactions involving a nearest atom n layers away from a Δ_n process are classified as nearest-neighbor ejections (NNE). Nearest-neighbor ejections can also be classified as either direct or grazing. Direct processes are head-on collisions, which are generally very efficient in transferring momentum. Grazing events are nearest-neighbor interactions, which do not involve direct impact in the final collision leading to ejection.

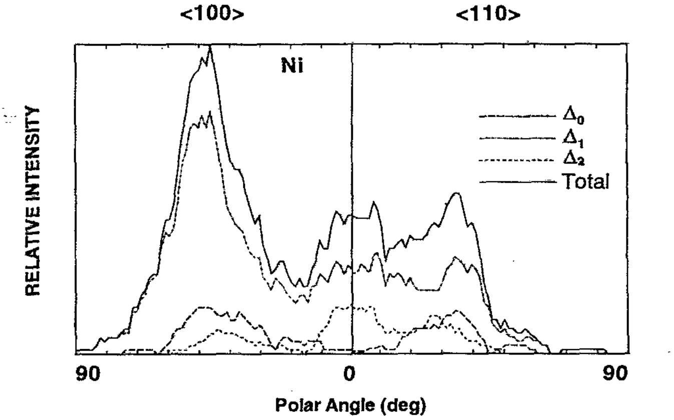

FIG. 7. Mechanistically resolved angular distributions for Ni along the ⟨100⟩ azimuth (left) and for the ⟨110⟩ direction (right). Each subdivision is labeled in the legend.

The grazing processes typically transfer momentum less efficiently than the direct collisions. There are also non-nearest-neighbor ejections (non-NNE) or channel processes. Non-NNE events are Δ_n processes in which the initiating atom, n layers away from the ejecting atom, is not the closest possible nth layer atom (with respect to the equilibrated lattice). This category accounts for the momentum transfer, which occurs when a highly energetic particle moves through the lattice initiating the motion of many atoms, often many lattice units from its initial position in the lattice.

The angular distributions of particles ejected via these mechanisms along both the ⟨100⟩ and the ⟨110⟩ azimuthal directions are shown in Fig. 8 for the Δ_1 processes. The particles that eject via grazing interactions are not peaked and make a significant contribution to the overall ejection yield. Direct nearest-neighbor events are largely responsible for the off-normal peak displayed in the angular distributions along the ⟨100⟩ direction, but are more evenly distributed at the angles of interest in the ⟨110⟩ azimuth. The non-NNE events contribute both to the normal and the off-normal peak along both azimuths. With respect to the energy dependence of the Δ_1 contri-

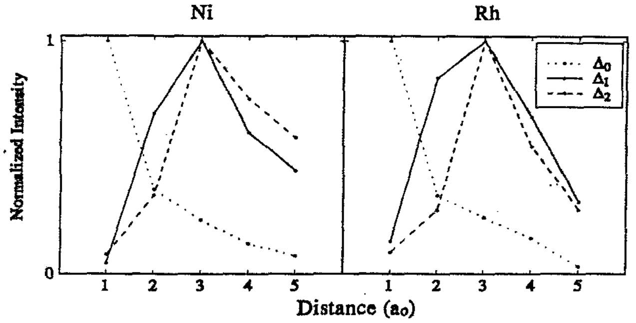

FIG. 6. Peak normalized distributions of intensity of the various Δ processes, as a function of the ejecting particles original distance from the origin of the impact zone. The dotted line corresponds to the Δ_0 mechanisms, the solid line represents Δ_1 processes, and the Δ_2 events are plotted using a dashed line. Lines are drawn simply to connect data points.

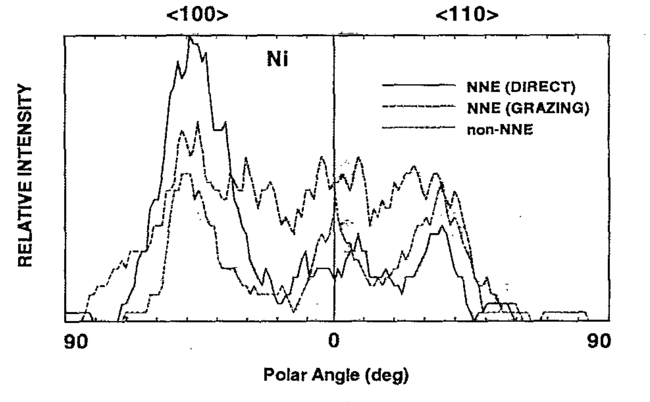

FIG. 8. Simulation results for ⟨100⟩ azimuth (left) and for the ⟨110⟩ direction (right). The angular spectra for each of the mechanistic subdivisions of the Δ_1 class. Each subdivision is labeled in the legend.

bution to the peak normal to the surface, we find that NNE events are responsible for the 5–10-eV contribution and non-NNE events are responsible for the 20–50-eV normal ejection. For Rh, there is no non-NNE contribution in the 20–50-eV range, presumably because the larger Rh size makes channeling between layers less probable.

The direct NNE events resemble Silsbee focusons[4] although we assign direct nearest-neighbor ejections of any chain length to this category. The average chain length for a direct Δ_1 for Ni is approximately two-nearest-neighbor units (<5 Å). Direct processes with chain lengths greater than two neighbor units are responsible for less than 10% of the ejections.[47] Grazing ejections, on the other hand, have significant chain lengths of momentum transfer through the lattice. This minimal contribution of focused ejection sequence asserts that the innate registry of the first few layers of the surface is the primary factor in determining the obtained macroscopic observables.

V. SUMMARY AND CONCLUSIONS

Energy-resolved angular distributions of Ni and Rh atoms, which desorb in the $^3D_3$ electronic state as the result of 5-keV Ar^+ bombardment of Ni{001} and Rh{001} have been experimentally measured and compared to molecular-dynamics computer simulations, which use the MD/MC-CEM interaction potential. The experimental spectra for the two elements are almost identical implying that the crystal and surface structure dominate the ejection process. The small differences in intensity are understandable in terms of the slightly different peak positions in the energy distributions. All features in the experimental spectra are reproduced in the calculated distributions. Second-layer atoms are found to eject preferentially along the normal direction and be largely responsible for the intensity at $\theta \leq 10°$. We find that at least three major ejection mechanisms exist for this surface. The dominant mechanism of ejection is one in which an atom in the layer below energies the atom of interest causing it to eject. Atoms ejected due to this mechanism are responsible for the major peak in the angular spectra. Collisions involving atoms in the same layer give rise to a shift in the peak position. The three main ejection mechanisms have been further categorized and the relative contributions of each has been presented. Furthermore, we have discussed the dependence of mechanistic composition of the main angular features as a function of the particles kinetic energy. Based on the results of this investigation we can predict, for a given energy and polar angle of ejection, what are the most probable mechanistic contributions for the feature in question. This study also strongly reinforces the view that the inherent registry of the atoms in the crystal lattice is the crucial factor in determining the dominant microscopic sequences of events, which lead to ejection as well as the macroscopically observable quantities of interest. This ability to quantitatively determine and predict the evolution of momentum transfer during the sputtering process is significant, with respect to simplifying our present understanding of the massively complex ejection process.

ACKNOWLEDGMENTS

We would like to express our appreciation to E. J. Dawnkaski, R. S. Taylor, R. Bhatia, R. Chatterjee, D. E. Riederer, and K. B. S. Prasad for their various contributions to this work. The financial support of the U. S. Office of Naval Research, U. S. National Science Foundation, the SUR program of the IBM Corporation and the M. Curie-Sklodowska fund No. NSF-93-144 is greatly appreciated. One of us (S. W. R.) would like to express thanks to C. L. Cobb and J. E. Coleman for their influence on this work.

---

[*] Also at Horizon Systems, 85 Old Long Ridge Rd., Stanford, CT 06903.

[1] G. K. Wehner, J. Appl. Phys. **26**, 1056 (1955).

[2] M. T. Robinson, in *Sputtering by Particle Bombardment*, edited by R. Behrisch (Springer-Verlag, Berlin, 1981), p. 73.

[3] Wehner's first experiments used glass plates to collect desorbed species. Material concentrated on the plates along specific directions of ejection in characteristic spots thus the angular distributions were termed spot patterns.

[4] R. H. Silsbee, J. Appl. Phys. **28**, 1246 (1957).

[5] D E. Harrison, J. P. Johnson, and N. S. Levy, Appl. Phys. Lett. **8**, 33 (1966).

[6] C. Lehman and P. Sigmund, Phys. Status Solidi **16**, 507 (1966).

[7] D. E. Harrison, P. W. Kelly, B. J. Garrison, and N. Winograd, Surf. Sci. Lett. **76**, 311 (1978).

[8] M. Hou and W. Eckstein, Nucl. Instrum. Methods Phys. Res. Sect. B **13**, 324 (1986).

[9] M. Hou and W. Eckstein, Phys. Rev. B **42**, 5959 (1990).

[10] R. Madoudian, Z. Postawa, M. El-Maazawi, B. J. Garrison, and N. Winograd, Phys. Rev. B **43**, 7311 (1990).

[11] N. Winograd, J. Chem. Phys. **96**, 6880 (1992).

[12] R. Bhatia and B. J. Garrison, J. Chem. Phys. **100**, 8437 (1994).

[13] R. P. Webb and D. E. Harrison, Jr., Nucl. Instrum. Methods Phys. Res. B **218**, 727 (1983).

[14] D. E. Harrison, Jr. and C. B. Delaplain, J. Appl. Phys. **47**, 2252 (1976).

[15] N. Winograd, B. J. Garrison, and D. E. Harrison, Jr., J. Chem. Phys. **73**, 3473 (1980).

[16] B. J. Garrison, J. Am. Chem. Soc. **102**, 6553 (1980).

[17] B. J. Garrison, N. Winograd, and D. E. Harrison, Jr., J. Chem. Phys. **69**, 1440 (1979).

[18] S. P. Holland, B. J. Garrison, and N. Winograd, Phys. Rev. Lett. **43**, 220 (1979).

[19] C. C. Chang, Phys. Rev. B **48**, 12 399 (1993).

[20] M. H. Shapiro and T. A. Tombrello, Nucl. Instrum. Methods Phys. Rev. Sect. B **84**, 453 (1994).

[21] D. E. Sanders, K. B. S. Prasad, J. B. Burnham, and B. J. Garrison Phys. Rev. B **50**, 5358 (1994).

[22] P. H. Kobrin, G. A. Schick, J. P. Baxter, and N. Winograd, Rev. Sci. Instrum. **57**, 1354 (1986).

[23] D. E. Harrison, Jr., CRC Crit. Rev. Solid State Mater. Sci. **14**, 51 (1988).

[24] B. J. Garrison, Chem. Soc. Rev. **21**, 155 (1992).

[25] B. J. Garrison, N. Winograd, and D. E. Harrison, Jr., J. Chem. Phys. **69**, 1440 (1978).

[26] B. J. Garrison, N. Winograd, D. M. Deaven, C. T. Reimann, D. Y. Lo, T. A. Tombrello, and M. H. Shapiro, Phys. Rev. B **37**, 7197 (1988).

[27] D. N. Bernardo, R. Bhatia, and B. J. Garrison, Comput. Phys. Commun. **80**, 259 (1994).

[28] M. S. Stave, D. S. Sanders, T. J. Raeker, and A. E. DePristo, J. Chem. Phys. **93**, 4413 (1990).

[29] T. J. Raeker and A. E. DePristo, Int. Rev. Phys. Chem. **10**, 1 (1991).

[30] E. Clementi, IBM J. Res. Dev. Suppl. 9, (1965).

[31] P. S. Bagus, T. L. Gilbert, and C. J. Roothan, J. Chem. Phys. **56**, 5159 (1972).

[32] M. Schmidt and K. Ruedenberg, J. Chem. Phys. **71**, 3951 (1979).

[33] D. E. Sanders, M. S. Stave, L. S. Perkins, and A. E. DePristo, Comput. Phys. Commun. **70**, 579 (1992).

[34] C. L. Kelchner, D. M. Halstead, L. S. Perkins, N. M. Wallace, and A. E. DePristo, Surf. Sci. **310**, 425 (1994).

[35] In contrast to the other elements, the experimental data for Rh_2 are less certain. The embedding function fit only to the bulk properties predicts that $D_e = 2.42$ eV and $r_e = 2.29$ Å for the dimer.

[36] M. S. Daw and M. I. Baskes, Phys. Rev. Lett. **50**, 1285 (1983).

[37] M. S. Daw and M. I. Baskes, Phys. Rev. B **29**, 6443 (1984).

[38] S. M. Foiles, M. I. Baskes, and M. S. Daw, Phys. Rev. B **33**, 7983 (1986).

[39] A. Wucher and B. J. Garrison, Surf. Sci. **260**, 257 (1992).

[40] The unscaled Firsov screening length was used. The complete Moliére equation is given in D. J. O'Connor and R. J. MacDonald, Radiat. Eff. **34**, 247 (1977).

[41] This terminology dates back to at least 1977, when we inherited the computer code from D. E. Harrison, Jr.

[42] In total, the energy and angular distributions of seven states ($^3F_{4,3,2}$, $^3D_{3,2,1}$, and $^1D_2$) have been measured. The $^3F_4$ state is the gas phase ground state, but we believe that the first excited state $^3D_3$ is more representative of the initial state of the metal solid. [C. He, Z. Postawa, S. W. Rosencrance, R. Chatterjee, B. J. Garrison, and N. Winograd (unpublished)]. In fact, within the resolution of the discussion presented here, all seven states have similar angular distributions. A more complete discussion of the energy and angular distributions will be presented later.

[43] R. Maboudian, Z. Postawa, M. El-Maazawi, B. J. Garrison, and N. Winograd, Phys. Rev. B **42**, 7311 (1990).

[44] D. E. Harrison, Jr., P. W. Kelly, B. J. Garrison, and N. Winograd, Surf. Sci. **76**, 311 (1978).

[45] M. H. Shapiro, P. K. Haff, T. A. Tombrello, D. E. Harrison, Jr., and R. P. Webb, Radiat. Eff. **89**, 234 (1985).

[46] P. J. Schmitz, W. Y. Leung, G. W. Graham, and P. A. Thiel, Phys. Rev. B **40**, 11 477 (1989).

[47] S. W. Rosencrance, Z. Postawa, B. J. Garrison, and N. Winograd (unpublished).